

AperTO - Archivio Istituzionale Open Access dell'Università di Torino

## Chitosan crosslinked flat scaffolds for peripheral nerve regeneration

### **This is the author's manuscript**

*Original Citation:*

*Availability:*

This version is available <http://hdl.handle.net/2318/1625674> since 2017-02-24T11:28:18Z

*Published version:*

DOI:10.1088/1748-6041/11/4/045010

*Terms of use:*

Open Access

Anyone can freely access the full text of works made available as "Open Access". Works made available under a Creative Commons license can be used according to the terms and conditions of said license. Use of all other works requires consent of the right holder (author or publisher) if not exempted from copyright protection by the applicable law.

(Article begins on next page)





**Abstract**

Chitosan (CS) has been widely used in a variety of biomedical applications, including peripheral nerve repair. Due to its excellent biocompatibility, biodegradability, stability, availability, and antifouling activity, in this study, CS hydrogels crosslinked with chitosan sulfonic polyacrylate (SDSP) alone (CS/SDSP) or in combination with γ-poly(D-glutamic acid)/methacrylate chitosan (CS/GPTMS/SDSP) were fabricated with a wet-spin casting technique. The crosslinking ratio of crosslinking agent and CS was precisely adjusted to obtain a composite material having both adequate mechanical properties and high biocompatibility. In vitro cytotoxicity tests showed that both CS hydrogels allowed cell survival and proliferation. Moreover, CS/GPTMS/SDSP membranes promoted cell adhesion, induced Schwann cell-like morphology and supported neurite outgrowth both in vitro and in vivo. Preliminary in vivo tests carried out on both types of nerve scaffolds (CS/SDSP and CS/GPTMS/SDSP membranes) demonstrated that provided for: (i) promoting, as a membrane, the rate of nerve conduction by end-to-end surgery and avoiding post-operative nerve adhesion; (ii) helping, as a scaffold, the two nerve segments after a nerve peripheral nerve lesion with 10% difference time. A long gap rat median nerve was repaired using CS/SDSP and CS/GPTMS/SDSP conductors to further investigate their ability to induce nerve regeneration in vivo. CS/GPTMS/SDSP tubes revealed to be more highly biocompatible and, using a 12-week post-operative layer of time, they showed from the distal nerve segment. On the contrary, CS/SDSP conductors presented more than 50% regeneration and functional recovery leading to an outcome comparable to median nerve repaired by autograft.

**Key words:** Polyphased nerve repair; regeneration; fibrillation; chronic Schwann cells.

## 1. Introduction

Polyphased nerve transection due to car accidents, sport and military injuries [1] are reported to affect, annually, more than one million people worldwide.

The possibility to repair nerve function is dependent on the severity of the damage sustained. Spontaneous recovery is possible only if the continuity of the nerve is maintained. In case of complete nerve transection, a suture is required for re-establishing a continuity between the proximal and the distal stumps. Autologous nerve grafts (anastomosis) is the "gold standard" technique for repairing peripheral nerve defects and is essential in the case of healthy nerve. Regrowth of sensory origin sensory the axonal nerve (for holding the grip) [2].

However, the practice presents some disadvantages: it requires an additional incision for harvesting the healthy sensory nerve, leading to a sensory deficit, yet, graft material is limited especially in case of an extended nerve lesion. In an alternative, a variety of biomaterials for nerve reconstruction has been developed [3-6]. In particular, chitosan (CS), as a natural polysaccharide, has recently attracted more and more attention due to its good biocompatibility, biodegradability, non-toxicity, ready availability and easy physicochemical properties [3-6].

Recent in vitro studies revealed the capability of CS membranes as substrate for survival and neuronal Schwann cell (SC) growth [7] as well as survival and differentiation of neuronal cells [8, 9].

CS-based biodegradable scaffolds have been widely used for neural repair in different animal models [10]. CS-based nerve conduits, alone or in combination with other biomaterials, have been found to bridge effectively peripheral nerve defects [11-13]. In CS nerve guides applied with the introduction of a biophysical CS membrane were used to reconstruct 10 mm sciatic nerve defects in adult healthy and diabetic rats, demonstrating an enhancement in functional and morphological nerve regeneration [14].

Standard nerve regeneration of long gaps has also been reported when CS cables are combined with poly(urea and poly(urea and adipate) (PU) functionalized poly(pyrrolone) (44) (54). Because pure CS is brittle and adipate supply (51,58), improved techniques and different crosslinking methods have been developed to overcome the poor mechanical strength of CS nerve grafts formed under physiological conditions, which is one of the main factors limiting the CS use in clinical applications for neurological and non (56).

In the present work, ethacrynic phosphate (EHP) and poly(ethylene glycol) diacrylate (PEG-DIAC) crosslinked CS for scaffolds, previously characterized in terms of physicochemical, mechanical, morphological, mechanical properties (59), were evaluated in terms of biological properties using in vitro and in vivo tests.

In vitro studies on RTG DAPIF cells were performed on adaptable CS based flat scaffolds to evaluate biocompatibility and to assess their potential applicability as nerve repair scaffold. In addition, CS flat scaffolds and conduits were tested *in vivo* in the model of rat median nerve repair. The outcome of nerve reconstruction was assessed at 12 weeks post-implantation through a combination of functional assessment, histological and morphological investigation.

## 2. Methods

### 2.1 Membrane preparation

CS membrane substrate weight 70%-85% divinylbenzene degree, Sigma Aldrich) was dissolved in acetic acid solution 0.5M at room temperature by continuous stirring to obtain a 2.5 % (w/v) solution. Crosslinked membranes were prepared according to the method previously described by Rami and colleagues [20]. Briefly:

1. DSP-entrained samples (CS/DSP) were obtained by adding DSP (10 (one drop per second) to the CS solution with a concentration of 7.5 % v/v with respect to the actual polymer solution volume. The mixed solution was kept under stirring at room temperature for about 10 minutes.

2. CS/DSP/DSP-entrained samples (CS/GPTMS)\_DSP were obtained adding GPTMS (0.5% w/v) to the CS solution. The resulting CS/GPTMS solution was kept under stirring for 1 hour followed by the dispersive addition (one drop per second) of DSP (10 (concentration 7.5 % v/v) and maintained under continuous stirring for 10 minutes.

Finally, 10 ml of each solution (CS/DSP and CS/GPTMS)\_DSP) were poured into a cast Petri dishes and co-dried for 48 h to obtain flat membranes. All crosslinked disk samples were dipped into demineralized water for 10 minutes and then the water pH values were measured to evaluate the presence of acidic residues.

Finally wet were performed by the authors, on CS/DSP and CS/GPTMS)\_DSP membranes, both in dry and in wet conditions [20].

### 2.2 In vitro cell tests on CS based membranes

In vitro cell tests were performed using BHK-212F1, a heterotetraploid cell line (ATCC - catalog number CRL-2730). Cytotoxicity tests were carried out on both CS/DSP and CS/GPTMS)\_DSP while, MTT-DHBT adhesion, proliferation and gene expression were evaluated on CS/GPTMS)\_DSP due to the

higher mechanical stability of the filament under physiological conditions and because they were considered as "the most pure" filamentous myofibrils for CSEPTIN\_DSP fibrillogenesis from the case of CSEPTIN supplemented with GPTM3. Native myofibrils of about one  $\mu\text{m}$  length (IMG) cultured in CSEPTIN\_DSP was discontinued by control of their microscopy.

### 2.2.1 Cryomicroscopy on CSEPTIN\_DSP and CSEPT

The effect of the CS based material context was studied as MYOBIOTY CSEPT and CSEPTIN\_DSP samples were incubated with a 20 minutes exposure to ultraviolet (UV) irradiation (UV lamp wavelength 254 nm, Schottmerck, Co., St. Louis, MO - Uppsala, Sweden). Material context were prepared by incubating both crystallized CS based myofibrils in Dubowitz's Modified Eagle Medium (DMEM, Sigma Aldrich) supplemented with 100 IU/ml penicillin (Sigma), 0.1 mg/ml streptomycin (Sigma), 5 mM sodium-pyruvate (Sigma), 4 mM L-glutamine (Sigma) and 10% heat-inactivated fetal bovine serum (FBS, Gibco Technologies) and stored at 37 °C in a humidified atmosphere of 5% CO<sub>2</sub> for 15 days. As control media, samples of culture medium were incubated in the same conditions of CSEPT and CSEPTIN\_DSP samples and then collected after 15 days. This procedure was used to test the use of the control on using cultured media. In detail, MYOBIOTY cells were seeded and cultured in the previous prepared control media, at a density of 2x10<sup>5</sup> cells/ml in 96-well dishes. After 2, 3, 5, and 7 days in vitro (DIV) cells were trypsinized and counted in a Beckman's flow cytometer chamber. Experiments were performed on technical replicates. The counts obtained from average were analyzed, averaged and expressed in logarithmic scale of cells culture (x 10<sup>3</sup>).

### 2.2.2 GFP infection on CSEPTIN\_DSP myofibrils

Immunocytochemistry analysis was performed on specifically cultured cell adhesion and morphology. R5-DMP7 were seeded at a density of  $1 \times 10^5$  cells/ml on microcarrier and control glass slides. After 24 hours of culture, culture medium was removed, substrates with attached cells were rinsed with PBS and fixed by the addition of 4% paraformaldehyde solution (PFA, Sigma-Aldrich). After 20 min the PFA was removed and each plate was washed with PBS. Fixed cells were permeabilized with 0.1% Triton X-100 and blocked with 1% Normal goat serum in 0.05M PBS (pH 7.4) for 1 h at room temperature. F-actin was detected using TRITC-conjugated phalloidin (Fluorolab) in blocking solution (Chemicon/Millipore) by 1 h incubation at room temperature. Following three wash steps of 5 min each, Vectastain was detected by overnight incubation with streptavidin-mouse-anti-rabbit IgG (Jackson ImmunoResearch) followed by 1 h incubation with goat anti-mouse Alexa 488 secondary antibody (Invitrogen/ThermoFisher) in 0.05M PBS.

A quantitative evaluation of the morphology of the cells plated on different substrates was conducted, taking into account the diameter and height of filopodia. The value of diameter of cultured cells was expressed as a percentage of total cultured cells in each experimental group. All the fluorescently-labeled cells were measured under a LSM 510 confocal laser microscopy system (Zeiss, Axio), which incorporates two beam (argon and HeNe) and is equipped with an inverted Axiovert 100 SB microscope.

### 3.2.3. Proliferation assay on C56F10SP\_01SP microcarrier

R5-DMP7 cells were seeded in 96-well microcarrier (96 F96, at a density of  $1 \times 10^5$  cells/ml) on both C56F10SP\_01SP and glass control plates (control). After 1, 3 and 5 days, culture medium was removed, substrates with attached cells were rinsed with PBS and fixed by the addition of 4% PFA. After 20 min, PFA was removed and each plate was washed with PBS. R5-DMP7 cells were stained with 1% crystal violet in deep purple buffer. At the same solution in 200  $\mu$ l from substrate (pH 9) for



GAGACCTGGAGACTTGG-362 Forward Sequence-CTAGTCAAGCCCTGAG-361 Reverse Sequence-GGCCAGGAGTCCCAAGAG-364 Forward Sequence

GAGGCGCTTATCAGAG-363 Reverse Sequence-GAGGACAGGGCAAGC-364 Forward Sequence-TCCTCTGTCAGAGGAGGAG-365 Reverse Sequence

GCTTCTGACAGAGAGAGAGGAGG-366 Forward Sequence-CTACCAAGAGAGGTCACAGAG-367 Reverse Sequence-CCGACACAGCAAGAGAG-368 Forward Sequence

GATCAAAACAGAGATGTCCTC-369 Reverse Sequence-GGGGAGAGTTCGAAAGGCTC-370 Forward Sequence

For identification in multiple sequencing genes, oligonucleotide primers C (180) and 524A binding primers (BP) were used. The reaction mixture (200 µl) included 7.5 µg genomic DNA and reverse primers.

1.25 µl SYBR Green II (Bio-Tek) and 5 µl dH<sub>2</sub>O. The PCR conditions were as following: initial step at 95°C for 2 min, then 40 cycles at 40°C for 20 s, and 40°C for 1 min. The results were obtained from three independent experiments.

**2.2.3. Total protein extraction, and western blot**

Total proteins were extracted by adding cells in boiling Lysosomal buffer (2.5% SDS and 0.125 M Tris-HCl pH 6.8, followed by 2 min at 100°C. Protein concentrations were determined by the BCA method, and equal amounts of protein (determined at 100°C in 100 µM 2-mercaptoethanol and 10% glycerol) were loaded into each lane, separated by SDS-PAGE, transferred to a HybondE-CL Extra membrane and blocked for 1 h at 37°C in 1% TBST (1% and NaCl), at pH 7.5 (pH 7.5), and 0.1% Tween-20/1% casein/10% milk. Membranes were incubated overnight at 4°C in primary antibodies diluted in TBST plus 1% casein/10% milk. The day after, they were rinsed four times with TBST for 3 min each at room temperature and incubated for 1 h at room temperature with peroxidase-labeled secondary antibody diluted in TBST plus 1% casein/10% milk. Membranes were washed 6 times, 5 min each, with

TEB is a non-proprietary and specific finding was detected by the national identification system (ICL system (American Biochemicals) using HighSpeed™ (American Biochemicals)).

Primary and secondary antibodies used are: rabbit polyclonal anti-B2C (1:500, n=45), Santa Cruz Biotechnology, Santa Cruz, CA, USA; mouse monoclonal anti-actin (1:1000, MAB316, Sigma). Immunoblot procedure (ECL) using anti-alkaline phosphatase antibody (1:10000, American Biochemicals) (Abp) and mouse secondary antibody (1:10000, American Biochemicals).

#### 2.2.6. Western immunoblot assay on CSOP/DMG\_SDP

DMG explants were harvested from adult female Wistar rats, weighing approximately 200 g, cultured and maintained in DMG's culture medium (DMG) for 1 hour under sterile conditions. Rat was sacrificed by a lethal ip injection of chloralhydrate + urethane according with the local Ethics Committee and the European Communities Council Directive (2003/63/EC). Adipogenic precursors were able to maintain gene and differentiate along into several brown adipocytes for culture, cell sorting and cloning.

DMG explants were cultured into differentiation medium (DMG) (American Biochemicals) and CSOP/DMG\_SDP for 48 hours and incubated at 37 °C for 1 hour. The medium was filtered (1) in the culture medium. Explants were incubated for 4 days in culture medium for medium (DMG) at 37 °C with 5% CO<sub>2</sub> supplemented with 10 ng/ml rTGF- $\beta$ 1. After 4 days, explants were fixed with 4% PFA for 15 minutes at room temperature. For immunofluorescence, briefly, the specimens were incubated overnight in a solution containing both anti-mouse- $\beta$ actin (monoclonal mouse 1:200, Sigma), and anti-porcine polyclonal anti-B2C (1:1000, American Biochemicals) primary antibodies. After washing in PBS, double immunolabeling was carried out by incubating sections for 1 h in a solution containing two secondary antibodies: anti-rabbit IgG (Cy3) (Jackson ImmunoResearch Laboratories) and anti-mouse IgG (Alexa Fluor 488 conjugated) (Molecular Probes). All samples were observed with a LSM 510

conditioned reflexology system (Elex, Stim), which incorporates two laser diodes and LED's and is equipped with an internal Arduino 103M microcontroller.

### 2.3 In vitro work on CNGP2<sup>+/+</sup> and CNGP2<sup>-/-</sup>

All procedures were approved by the Scientific Committee of the University of Torino, by the Institutional Animal Care and Use Committee of the University of Torino, and by the Italian Ministry of Health, in accordance with the European Committee Directive 2003/63/EEC.

#### 2.3.1 Animals and surgery

In vivo preliminary analysis were performed under general anaesthesia in 2 adult female Wistar rats, weighing approximately 200 g, in order to evaluate behaviour, variability and the possibility of their use for peripheral nerve injury. Before using C3 microstimulation, rats were anaesthetized by 5% isoflurane and placed in a supine position in the range of 10-15 cm. In the first case, the C3 microstimulation was used to map cranial median nerve and was closed with a suture point (Figure 1 A,B). In the second rat, the C3 microstimulation was closed up and glued with biological cyanoacrylate glue to obtain a long channel (Figure 1 C,D). Median nerve was transected, 3 mm of median nerve was removed and CNGP2<sup>+/+</sup> and CNGP2<sup>-/-</sup> DRG nodes were isolated following the two nerve injury (Figure 1 E,H).

Two weeks later, the median nerve was reconnected immediately after surgery.

**Microstimulation experiments were performed on the 32 adult female Wistar rats, weighing approximately 200 g, with either CNGP2<sup>+/+</sup> and CNGP2<sup>-/-</sup> DRG microstimulation, and up to 100 µm of peripheral nerve, and up to 100 µm of median nerve (Figure 1).**

The animals were divided by three experimental groups of 4 animals each for two groups, the median nerve was transected and repaired with CNGP2<sup>+/+</sup> or CNGP2<sup>-/-</sup> axons. Median nerve repaired with nerve allograft was used as control. The surgical procedure was previously described by Yu and colleagues [21]. The complete and

The animals were adapted during their 4-week period of acclimatization to the conditions of the experiment. In order to prevent interference with the growing test device during testing due to the use of the conventional bedding, the conventional bedding was removed at the middle third of the backbones and its presence was reduced to the minimum major extent to avoid spontaneous combustion [2]. After 12 weeks post-operation, rats were sacrificed and organometal levels analyzed.

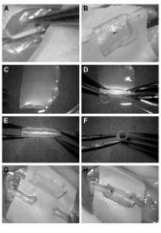


Figure 1. (A) Turbine in the middle, (B) (C) turbine and in the middle, (D) turbine, (E) (F) turbine and in the middle, (G) turbine and in the middle, (H) turbine and in the middle, (I) turbine and in the middle, (J) turbine and in the middle, (K) turbine and in the middle, (L) turbine and in the middle, (M) turbine and in the middle, (N) turbine and in the middle, (O) turbine and in the middle, (P) turbine and in the middle, (Q) turbine and in the middle, (R) turbine and in the middle, (S) turbine and in the middle, (T) turbine and in the middle, (U) turbine and in the middle, (V) turbine and in the middle, (W) turbine and in the middle, (X) turbine and in the middle, (Y) turbine and in the middle, (Z) turbine and in the middle.

### 2.1.2 Fluorescence assessment of chemical markers

Clipping test sections were carried out every 15 weeks until week 12. Clipping test was performed following the same procedure previously described (22) using the BS-Grip Grip Meter (Orthopedic Instruments, Vienna, Italy). The test is carried out by holding the test by the tail and lowering it towards the device and then, when the animal grips the grid (making it descend until it hits its grip). When the marker wears down it is required the animal's paw approaches the grid in a single, rapid extension. The behavior records the maximum weight that the animal manages to hold up before losing the grip. Each animal was tested three times and the average value was recorded. Since assessment of animal welfare was one of the main objectives of the study, a careful daily animal care/behavior was adopted for posture and action measurement, under standardized and quiet conditions, especially during early post-operative times.

### 2.1.3 Immunohistochemistry and confocal laser microscopy

Frontal sections, the entire cornea, with adjoining Descemet's folds, were frozen, cut and analyzed with immunofluorescence or confocal laser microscopy. Series of 10-20  $\mu\text{m}$  thick, longitudinal sections were cut by a Cryostat (Leica Microsystems, Wetzlar, Germany). Sections were then incubated overnight in a solution containing anti-mouse/anti-rabbit primary antibody (conjugated, mouse, which recognizes the 200 kDa subunit of  $\alpha$ -tubulin/actin, dilution 1:200, Sigma) and then, after washing in PBS, incubated for 1 hour in a solution containing Alexa488-conjugated anti-mouse IgG1 solution (1:500, Life technologies). The sections were finally mounted with a DAPI fluorescent mounting medium and analyzed by a LSM 1010 confocal laser microscopy system (Leica, Jena, Germany).

### 2.1.4 Brisk embedding and electron microscopy

After the 12-week follow-up this material was recombined and the nerve segment fixed in the osmium tetroxide, fixed and prepared for design-based stereological analysis of myelinated nerve fibers and for electron microscopy. Nerve samples were fixed by immersion immersion in 2.5% perfused glutaraldehyde and 0.5% osmium in 0.1 M Tris-cacodylate buffer for 4 h. Specimens were then washed in cacodylate containing 1.5% osmium in 0.1 M Tris-cacodylate buffer, post-fixed in 1% osmium tetroxide, dehydrated and embedded in araldite. From each nerve section of white matter transverse sections (2.5 µm thickness) were cut starting from the distal stump of each myelinated nerve segment using an Ultramicrotome (Leica Microsystems, Wetzlar, Germany) and stained using Trichrome blue for high resolution light microscopy examination and design-based stereology. For transmission electron microscopy ultrathin sections (100-150 nm thick) were cut using the same ultramicrotome and stained with uranyl acetate solution of uranyl acetate and lead citrate. When thin sections were analyzed using a TEM 1000 transmission electron microscope (LEICA, Wetzlar, Germany).

### 2.1.1. Design-based quantitative morphology of nerve fiber representation

In each nerve segment that contained an LNMP axon, design-based stereological analysis was applied and using our randomly selected software three random variables section, A, DMS3000B microscope equipped with a DIC/DM digital camera and an SEMV image manager system (Leica Microsystems, Wetzlar, Germany) was used for stereology. The final magnification was 5000X, resulting in clear identification and unequivocal analysis of myelinated nerve fibers. The cross-sectional area from each nerve was randomly selected and the total cross-sectional area of the nerve was measured. The length of fibers in each nerve was then randomly selected using a previously described stereological method [25]. Two-dimensional diameter profiles were also used to which an additional representative sample of myelinated nerve fibers. Fiber number was calculated from fiber and area [6].

data were measured and the risk being observed of their (2) and none of them calculated. These data were used to calculate expected likelihood (3)–(5), and the ratio (2/3).

#### 2.4 Methods

For in vitro experiments, data were expressed as mean  $\pm$  SEM. Statistical analysis was carried out using single-factor analysis of variance (ANOVA) post hoc Bonferroni. Values of \* $p$ <0.05, \*\* $p$ <0.01, \*\*\* $p$ <0.001 were considered as statistically significant. For in vivo experiments data were expressed as mean  $\pm$  SD. Statistical analysis was carried out using Two-sample  $t$ -Test. Values of \* $p$ <0.05, \*\* $p$ <0.01, \*\*\* $p$ <0.001.

### 3. Results

#### 3.1 In vitro cell lines as CS benchmarks

##### 3.1.1 Cytotoxicity study on C56F10B\_02P and C56F10P

The effect of the CS based material release was evaluated by RTG-2 (RTG) proliferation assay counting the number of proliferating cells after 2, 5, 15 and 30 days (Table 1). RTG-2PCT showed the release of C56F10P and C56F10B\_02P showed no cytotoxic effect since no significant differences in cell number were detected between these two culture conditions and the control.

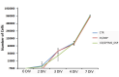


Figure 2. Evaluation of the effect of incubation period. Adhesion rate of R51-D807T cultured cells adhered to 1) and 2) control versus CS-GP130 and CS-GP130-DSP substrates.

#### 1.1.2 Cell adhesion on CS-GP130-DSP substrates

R51-D807T cells were seeded on CS-GP130-DSP and on control glass-immunocytochemistry analysis was performed after 24 hours of culture to specifically evaluate cell adhesion and morphology. In order to obtain a more detailed evaluation of cell adhesion, the cells cytoskeleton and focal adhesion complex were stained using TRITC-conjugated phalloidin and anti- $\beta$ -tubulin antibody, respectively. R51-D807T cells internalized and compared with CS-GP130-DSP substrates. Differences in morphology and size were observed when R51-D807T cells were cultured on control glass and CS-GP130-DSP (Figure 3). Cells on control glass displayed a higher rate; they were also more spread without particular orientation of the actin cytoskeleton (Figure 3A and C). Cells cultured on CS-GP130-DSP displayed a more elongated morphology characterized by a typical head-tail cell body with long protrusions, giving an overall spindle shape that is typical of SVs (Figure 3B and 3D).

The analysis of the morphology of these cells placed on different substrates showed that the cells of cells placed on control substrates (glass) presented a flattened form, similarly to fibroblasts, and only

DN as depicted above relative to SC. By contrast, 50% of the cells cultured on CSOPDM\_2MP had generated the SC-like elongated shape.

Viability immunostaining was performed to visualize the exact location of focal adhesion sites.

Viability-positive sites were observed on cells seeded both on control and CSOPDM\_2MP, but with different distributions. CSOPDM\_2MP membranes presented cells with a higher concentration of viabilities around the tracks (Figure 3F) while protein concentrations at the edges of cells was slightly elevated in control (Figure 3G).

#### 3.3.3. Proliferation assay on CSOPDM\_2MP membranes

Proliferation assay was performed on CSOPDM\_2MP samples (Figure 3G). R15-24027 cells were cultured on both CSOPDM\_2MP and glass plates (control). The number of proliferating cells was determined after 7 days (DN).

R15-24027 cells seeded on CSOPDM\_2MP showed lower proliferation rate and significant differences in cells numbers were detected in the culture conditions after 7 DIV (\*\*p<0.01) and 4 DIV (\*\*\*)p<0.001), in comparison to positive control. Yet, it was possible to observe a constant increase of cell numbers on CSOPDM\_2MP samples at each time point.

#### 3.3.4. Gene and protein expression of *WNT4* and *WNT5A* cultured on CSOPDM\_2MP samples

Both *WNT4* and *WNT5A* mRNA expression changes were evaluated to study progenitor and cell survival signaling after 7 and 4 days of culture of R15-24027 cells on CSOPDM\_2MP samples.

The relative values of *WNT4* and *WNT5A* mRNA expression were not significantly different when comparing CSOPDM\_2MP with control conditions, both after 7 and 4 days of culture. (Data not shown). By contrast, significant differences in the *WNT5A* mRNA expression was observed after 7 days of

which T<sub>H</sub>17s respond to the context although the difference was not observed after 6 days (Figure 1B).

The same pattern of expression was detected at the protein level: the decreased protein expression of IL-17 after three days of culture of the WT-DMP12 cells on thymus medullators, undergo a clear recovery after six days of culture, although not to the baseline values (Figure 1C).

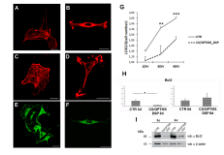


**Figure 1. Cell surface expression of cytokines.** (A) Intracellular expression of IL-17 in WT-DMP12 cells cultured on thymus medullators for 3, 6, and 9 days. (B) IL-17 mRNA levels in WT-DMP12 cells cultured on thymus medullators for 3, 6, and 9 days. (C) IL-17 protein levels in WT-DMP12 cells cultured on thymus medullators for 3, 6, and 9 days. (D) IL-17 protein levels in WT-DMP12 cells cultured on thymus medullators for 3, 6, and 9 days. Error bars represent standard deviation. \*p < 0.05, \*\*p < 0.01, \*\*\*p < 0.001.

### 3.1.1. Media and growth media for CSOPFNs\_DSP

DMEM medium was purchased from Gibco. Media was used and cultured for 4 days on overnight coated coverslips and CSOPFNs\_DSP for neurite outgrowth. The cultures were fixed and immunostained for NF-200. Media present and peripheral axons and then analyzed by laser confocal microscopy. A double labeling immunofluorescence revealed that both neuronal intermediate filament proteins were expressed by DMEM neurons (Figure 6).

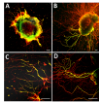


Figure 6. Laser confocal images showing double labeling of neuronal intermediate filament proteins of control neurons at 4 days after PBN exposure relative to neurons grown on coverslips (a, c) and CSOPFNs\_DSP for neurite outgrowth (b, d). Scale bar = 100 micrometers.

### 3.2. In vivo peripheral analysis

In order to evaluate neurotoxicity for peripheral nerve targets, the neurotoxicity of CSOPFN and CSOPFN\_DSP were tested in vivo in adult female Wistar rats.

Both neurotoxicity tests to be performed in PBN studies are to make it make them viable. Diagram can help size and shape of neurotoxicity depending on the size of the nerve and the lesion type and extent. They can be used to predict an injured nerve from adhesion (Figure 7B) or as a model to help a nerve defect (Figure 7C). Both neurotoxicity models to have a good neurotoxicity after the PBN immersion.

and the recovery for the six weeks post-surgery. Results are given in the appendix table, and they are only included up until about CSOPND, DSP, established by week four eight.

### 3.3 In vitro work with CSOPND, DSP and CSOPND, DSP and CSOPND, DSP

#### 3.3.1 Participants assessment of functional recovery

In vivo work requires participants to be carried out with both CSOPND and CSOPND, DSP conditions. The manual motion sensors of force were not used by either up and side-tilted CSOPND or CSOPND, DSP conditions. Manual motion sensors were just (temporarily) used in control.

Figure 5 reports the post-operative time course of functional recovery for six weeks using CSOPND and CSOPND, DSP. In the group of CSOPND, DSP conditions, functional recovery of finger force reaches 90% of pre-operative during of post-operative period. This observed to be due to the detection of CSOPND, DSP when force is detected in range.

The function of finger force muscle, measured by the motion sensors used to recover faster for subjects involving a performance markedly different from CSOPND at week 4 after injury (p<0.05). Functional recovery for CSOPND showed a week 4 and progressively increased. At week 8 and 12, no more significant differences were detectable between original and CSOPND treatment.



Figure 5. Post-operative time course of functional recovery for six weeks using CSOPND and CSOPND, DSP. In the group of CSOPND, DSP conditions, functional recovery of finger force reaches 90% of pre-operative during of post-operative period. This observed to be due to the detection of CSOPND, DSP when force is detected in range.

### 3.2.2 Immunohistochemistry and confocal laser microscopy

Axonal regeneration was analyzed by confocal laser microscopy on longitudinal nerve lesion sections after immunohistochemical staining (Figure 6). After 12 weeks post injury, the axonal expression of both C82FPM5, GFP and C82FPM5-GFP was greatly reduced in the nerve. C82FPM5, GFP and C82FPM5-GFP control distal nerve axons staining for axons, with distal axonal and synaptic vesicles in the C82FPM5, GFP control (Figure 6A) and finally control in C82FPM5 control (Figure 6B).



Figure 6. *In vivo* axonal regrowth evaluation. Transverse sections on longitudinal sections of 12 weeks control and C82FPM5, GFP and C82FPM5-GFP were greatly reduced in the nerve. C82FPM5, GFP and C82FPM5-GFP control distal nerve axons staining for axons, with distal axonal and synaptic vesicles in the C82FPM5, GFP control (Figure 6A) and finally control in C82FPM5 control (Figure 6B).

### 3.2.3 Light and transmission electron microscope analysis

Figure 7 shows high-resolution light and transmission electron microscope images of the distal rat median nerve injured, repaired with sutured or C82FPM5 control and harvested at 12 weeks post operation. Distal median nerve treated with C82FPM5, GFP was an increased axonal number, axons were found to be detached from the distal axonal site. Small myelinated axons and microtubules typical of regenerated nerve fibers were detected both in nerves repaired with sutured (Figure 7 A-C, E, G) and with C82FPM5 control (Figure 7B, D, F).



2.2.3. Single-blind, parallel, randomized, controlled trial of acute pain management  
 12-week post-operative, single-blind, randomized trial of regional analgesia versus regional with CSFOP sites or non-pain-therapeutic controls in terms of total number of analgesic doses (range 0–10) (CSFOP = 7.0 (0.1)), Ace and then diamine and Grate vs significantly more (p=0.01) in median doses compared with CSFOP sites when compared to analgesic, while morphine doses showed comparable results (p=0.05).

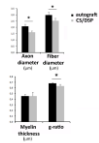


Figure 4. Mechanism of action of regional analgesia for acute pain management consisting of patients of analgesic doses and morphine doses. Data are presented as mean (SD) and error bars represent 1 SD. Significant differences between the two groups are indicated by asterisks (\*p<0.05).

#### 4. Discussion

Application of CS to bone engineering is a very novel and exciting topic [13,28]. This biomaterial's attractive not only for its high biocompatibility and biodegradability, but also for its anisotropic properties and the absence of immune response.

However, physical and mechanical properties of CS when it is associated with various solutions have to be carefully considered in order to apply it properly for regenerative purposes.

In the manuscript CS was treated with crosslinking agents able to act on its chemical/physical and mechanical properties, mainly  $\gamma$ -polyvinylpyrrolidone (PVP), ethane sulfonic phosphon (ESP) and a combination of PVP and ESP (PVP+ESP), as previously described by Boccia and colleagues [29].

**The present of PVP and ESP allowed that these agent was homogeneously distributed in the developed hydrogel and increased the water stability and the stiffness of CS/PVP, ESP and PVP+ESP.**

##### **Stiffness of CS/PVP hydrogel**

Both CS/PVP+ESP and CS/ESP the membranes were studied *in vitro* and *in vivo* for the implementation of CS-based nerve scaffolds.

First of all, the presence of degradation of the CS membranes, both CS/ESP and CS/PVP+ESP, showed no major effects on physical and mechanical properties.

Yet, preliminary analysis of glial cells number in CS/PVP+ESP membranes led to confirm that CS is capable to support glial cell proliferation [25] although delayed in comparison to previous studies.

This is attributable to the need for an initial adjustment in the new culture. The need of adjustment of the cells in the culture was demonstrated also by gene expression analysis of the cell progeny phase.

In CE that is significantly lower in the genes for 3 days on CS/PVP+ESP while the difference was no more detectable after 6 days.

The results of cell cultures in the C3GFPMS\_DBP conditions showed that cells with cytoskeletons of different morphology and actin and microtubule distribution, supporting the view that they cells have a higher migration capacity on the basement, a key requirement for the early stages of nerve regeneration [24]. The actin cytoskeleton is a highly dynamic network composed of actin polymer and a large variety of associated proteins. The function of the actin cytoskeleton is to maintain variety of essential biological functions, including intracellular and extracellular movement and structural support. The organization and distribution of actin filaments within a cell is, therefore, an important determinant of cellular shape, adhesion and motility [25].

The movement of the membrane of neurons with the neuronal cytoskeleton is a key pre-requisite step in evolution, in vitro, the potential for neural regeneration. Exponent of neuronal morphology (ENMG) is a valuable in vivo model to observe the neurite outgrowth in different substrates [26]. In our research, while ENMG was cultured on C3GFPMS\_DBP substrates and on glass, in control. After four days a high number of neurites sprouting from each of the control and control plates, was appreciated, on both substrates. Although quantitative analysis was not carried out, careful observation led to detect a greater spreading and neurite extension on the C3 substrate in comparison to control.

In preparation of in vitro experiments, a series of preliminary work allowed us to evaluate the permeability of C3 membranes. It was possible to establish the easy handling and the possibility to build at the time of the surgery a tube of specific size and shape depending on the nature of nerve damage, although it was evident that the C3GFPMS\_DBP is much more fragile in comparison with C3 itself.

Both C3GFP and C3GFPMS\_DBP conditions were used for bridging across 10 mm long rat median nerve defects, and the outcome of 12 weeks post-implantation was evaluated by functional, immunohistochemical and histological investigations. We observed that C3GFPMS\_DBP shows some drawbacks from the clinical setting (i.e. due to excessive fragility), and thus an alternative strategy

control. This result was confirmed by confocal laser microscopy which displayed very poor axonal representation with an irregular orientation inside Cx36/PTEN<sub>fl</sub> axons.

By contrast, Cx36<sup>fl</sup> axons showed functional recovery that started at week 4 and progressively increased reaching values similar to untreated controls at week 6. The delayed functional recovery is justified by the different repair techniques used in line with the results obtained using other types of axons [25].

Interestingly, morphological analysis showed distinct subtypes typical of regenerated nerve fibers with small nerve fibers at different regeneration stages and myelinated fibers. Though morphological analysis revealed that Cx36<sup>fl</sup> has, on average, smaller fibers than untreated.

#### F. Conclusions

In this work, we have achieved a histological quality similar to that of control for axonal morphology, biodegradability, axonal conductivity, and axonal activity. Considering previous low potential, axons will undergo mechanical properties for successful application in the field of peripheral nerve regeneration.

Our experience showed that Cx36<sup>fl</sup> could be a promising peripheral nerve regeneration with an outcome close to that reached by nerve autografts which are generally considered as the gold standard for treating severe nerve defects. These newly developed nerve guides should thus be regarded as promising alternatives to traditional nerve autografts.

However, it could be interesting to combine our obtained results with filling materials composed with growth factors [26] might be able to further increase the effectiveness of the scaffold device. Yet, creation of a 3D inner structure, which simulates extracellular matrix, might also provide a further support to axon and glial cells [21,22,33]. Therefore, although the device that we propose is simple

and any further changes. Some requirements should clearly indicate the functional behavior of the considered software when the further increase the operation period of the device.

#### Acknowledgments

The research was supported by Regione Piemonte - PIA di Innovazione - INCOGNITE project number 180/2017.  
The authors declare no conflict of interest.

**References**

1. Dai, W., Yan, Y., Ding, D., Wu, B., A. Patel, A. (2011) A hierarchical approach to peripheral neuropathic pain relief by peripheral nerve gap and continuous electrical current. *J. Neurosci.* 31: 1511-1520.
2. Grewal, A., Lurie, A., Pappas, M., Fawcett, J., Turner, D., et al. (2003) Effect of genetically modified Schwann cells with increased myelin on axonal nerve growth. *Neuroscience* 121: 427-432.
3. Li, F., Wang, X., Gao, Y., Wang, A., Wang, M. (2004) Transfection of peripheral nerves, bridging nerve gap after transection. *Neuroscience* 121: 1067-1076.
4. Katsuno, S., Fukuoka, M., Tan, F., Ratanasri, K., Goto, H., Kubota, M., et al. (2011) Perspectives in regenerative medicine: engineering of peripheral nerve with stem cell. *Cell* 145: 104-116.
5. He, H., He, T.T., Tang, D.C. (2012) Nanoparticle uptake and gene transfer efficiency for MSCs on oligodendrocyte Schwann cell-based Schwann cell transplantation. *Neuroscience* 211: 1021-1031.
6. Mochly, A., Elgarni, A., Mochly-Rosen, M., Mousavi, A., Mousavi, R.A. (2013) Schwann cell-based genetic therapy and Schwann cell transplantation: current state-of-the-art. *Neuroscience* 247: 101-112.
7. Yuan, X., Zhang, H., Song, Y., Wang, X., Gu, X. (2011) The interaction of Schwann cells with fibrous membranes. *Cell* 145: 1021-1031.
8. Datta, S., Kulkarni, R., Kulkarni, K., Shukla, M. (2005) Correlation of adhesion and degradation of fibrous membranes by Schwann cells. *Neuroscience* 131: 1021-1031.
9. Sano, M., Goto, A., Shimizu, Y., et al. (2011) Schwann cell-based Schwann cell transplantation in vivo Schwann cell transplantation using the peripheral nerve regeneration. *Neuroscience* 174: 141-151.
10. Grewal, A., Lurie, A., Pappas, M., Fawcett, J., Turner, D., et al. (2003) The use of Schwann cell-based Schwann cell transplantation in the mouse system. *Neuroscience* 119: 141-151.
11. Li, H., Yan, Y. (2011) PEG2-Archimedes cell-based Schwann cell transplantation for peripheral nerve regeneration. *Neuroscience* 174: 141-151.
12. Hwang, J.H., Kim, S., Kim, S., Kim, S., Kim, S., Kim, S., et al. (2011) Schwann cell-based Schwann cell transplantation for peripheral nerve regeneration. *Neuroscience* 174: 141-151.
13. Hwang, J.H., Kim, S., Kim, S., Kim, S., Kim, S., Kim, S., et al. (2011) Schwann cell-based Schwann cell transplantation for peripheral nerve regeneration. *Neuroscience* 174: 141-151.
14. Hwang, J.H., Kim, S., Kim, S., Kim, S., Kim, S., Kim, S., et al. (2011) Schwann cell-based Schwann cell transplantation for peripheral nerve regeneration. *Neuroscience* 174: 141-151.

15. Cheng SH, Wang J, Tang F, Cheng Y, Zhou X, et al. (2015) Dual cylindrical propeller and wave diffraction of composite thin film structures and grating structures. *Microstruct* 24: 2017-2047.
16. Wang M, Hu W, Cao Y, Liu Y, Wu J, et al. (2015) Dual axial wave propagation across a 3D meta-material by cylindrical grating structures. *Appl Phys Lett* 107: 191101.
17. Wang M, Xu Q, Wu Y, Gong M, Liu X, et al. (2015) Physical properties and biocompatibility of a porous copper-based thin film prepared using the wave propagation. *Microstruct* 24: 20-26.
18. Yang X, Gu X, Liu M, Hu W, Wang X, et al. (2016) Fabrication and properties of a porous copper-based thin film prepared using the wave propagation. *Microstruct* 24: 171-177.
19. An Q, Jiang Y, Fan H, Guo J, Zhu H, et al. (2015) The preparation of monolayer silver nanowire and its application in wave propagation control. *Appl Phys Lett* 107: 191101.
20. Xiao F, Xiao T, Chen Y, Chen Y, Chen H, et al. (2015) Chemical synthesis for linear propagating propagation of cylindrical structures. *Microstruct* 24: 101-107.
21. Xu F, Wang G, Nicholas S, Andric C, Kuznetsov A, et al. (2016) Enhancement of the linear wave propagation for the propagation of cylindrical wave propagation. *J Numerical Methods* 100: 100-117.
22. Xu F, Wang G, Nicholas S, Andric C, Kuznetsov A, et al. (2016) Chapter 4 Methods and results in numerical wave propagation. *J Numerical Methods* 100: 100-117.
23. Andric C, Wang G, Nicholas S, Andric C, Kuznetsov A, et al. (2016) Chapter 4 Methods and results in numerical wave propagation. *J Numerical Methods* 100: 100-117.
24. Andric C, Wang G, Nicholas S, Andric C, Kuznetsov A, et al. (2016) Chapter 4 Methods and results in numerical wave propagation. *J Numerical Methods* 100: 100-117.
25. Nataraja GV, Page SM, Venkatesh L, Ramesh M, Rama D (2016) Diffraction based up-coupling and filtering of propagating wave propagation. *Appl Phys Lett* 110: 141101.
26. Li Q, Zhou X, Zhou W, Zhang L, Wang C, et al. (2016) Porous silicon nanowire with surface plasmon resonance and photonic band structure. *Microstruct* 25: 101-107.
27. Chen YH, McEwen D, Cheng C, Mognetti B, Russell J, et al. (2015) Atom and electron cell propagation using wave propagation. *Phys Rev Lett* 115: 141101.
28. Johnson ME, Kipp MB, Andric C, Wang G, Wang H, et al. (2015) F-wave bands allow the control of wave propagation through cylindrical wave propagation. *J Appl Phys* 118: 101101.
29. Zhou X, Kuznetsov A, Fagnard J, Shalunov S, Kuznetsov A, et al. (2016) In vivo models for photonic wave propagation. *Appl Phys Lett* 109: 191101.
30. Gholami G, Farid D, Kuznetsov A, Kuznetsov A, Kuznetsov A, et al. (2015) Local delivery of the wave propagation through cylindrical wave propagation. *Appl Phys Lett* 108: 191101.

20. Mangan, M.; Winkler, S.; Nagendran, P.; Jha, S.; Ghosh, A., et al. (2014) Neurobiology of acute stress. *Journal of Neuroendocrinology* 36(1), 1-12.

21. Green, S.; Green, S.; Provencher, L.; De Rivecourt, D. (2013) Stress engineering and peripheral nerve regeneration: an overview. *PLoS One* 8(12), 1-11.

22. Green, S.; Provencher, L.; De Rivecourt, D.; Ghosh, A., et al. (2014) The influence of electrotopical stimulation on peripheral nerve regeneration: a review. *Journal of Neuroendocrinology* 36(1), 1-12.

23. De Rivecourt, D.; Ghosh, A.; Winkler, S.; Winkler, S. (2014) Designing ideal conditions for peripheral nerve repair. *Neuroscience Letters* 571, 1-12.